Brillouin light scattering investigation of dynamic spin modes confined in cylindrical Permalloy dots

G. Gubbiotti
Istituto Nazionale per la Fisica della Materia, Unità di Perugia, Via A. Pascoli, 06123 Perugia, Italy

G. Carlotti
Dipartimento di Fisica, Università di Perugia and Istituto Nazionale per la Fisica della Materia, Via A. Pascoli, 06123 Perugia, Italy

T. Okuno
Institute for Chemical Research, Kyoto University, Uji 611-0011, Japan

T. Shinjo
International Institute for Advanced Studies, Soraku-gun, Kyoto 619-0225, Japan

F. Nizzoli and R. Zivieri
Dipartimento di Fisica, Università di Ferrara, and Istituto Nazionale per la Fisica della Materia, Via Paradiso 12, I-44100 Ferrara, Italy

(Received 28 May 2003; revised manuscript received 24 July 2003; published 10 November 2003)

The quantized mode spectrum of standing spin waves and edge modes in cylindrical Permalloy dots with a radius R in the range between 100 and 500 nm, thickness $L=50$ nm, and separation $2R$, is examined from both experimental and theoretical points of view. Brillouin scattering measurements in the Damon-Eshbach geometry give evidence of a marked discretization of the spectra with respect to that of the continuous Permalloy film. The modes can be classified into two distinct families according to their frequency. The upper one consists of the usual Damon-Eshbach, dipole-exchange modes. The modes belonging to the lower family, instead, oscillate parallel to the applied field and are reminescent of the backward modes of the film. Brillouin measurements performed with the applied field parallel to the transferred spin-wave wave vector, confirm this interpretation. The frequencies of these waves have been calculated using a simple theoretical model including the exchange field. Also, a laterally confined mode belonging to this family is observed and its frequency is independent on the dot radius.

DOI: 10.1103/PhysRevB.68.184409 PACS number(s): 75.30.Ds, 75.75.+a, 78.35.+c

I. INTRODUCTION

In the last decade, thanks to the progress in lithographic techniques, it has become possible to fabricate ordered arrays of magnetic elements in the nanometer scale with enhanced physical properties which have no counterparts in bulk material and largely depend on the element shape and size.[1] Among these, the magnetization reversal dynamics at nanosecond time scales is an important subject for many technological applications of magnetic materials.[2] In the magnetic recording industry, the fast magnetization reversal in storage media and read heads is primordial to guarantee a high data transfer rate. Read and write speeds are today of the order of 300–400 MHz and are not limited by the magnetization reversal times. As these times will evolve towards the GHz regime, limitations due to magnetization reversal speeds can be expected because the finite lateral dimensions greatly influence the spin-wave spectrum, giving rise to discretization effects which are not observable in a continuous magnetic film.[3]

The shape induced modifications of the magnetostatic modes have been theoretically investigated since a long time ago. After the pioneering work of Walker[4] on magnetostatic modes in spheroidal samples magnetized along their axes, Fletcher and Kittel[5] gave the first derivation of the spectrum of magnetostatic spin waves in an infinite circular cylinder. A more general approach by Joseph and Schlömann[6] extended the calculation of magnetostatic mode frequencies to the family of volume modes in axially magnetized cylinders. A theory of normal mode frequencies in a sample of arbitrary shape based on a variational procedure was developed by Sparks.[7] On the other hand, an analysis of the absorption of microwave in a normally yttrium iron garnet (YIG) magnetized disk have been highlighted the characteristic of radially propagating waves and the related quantization effects.[8] Further calculations of resonant frequencies on rectangular thin films of YIG were performed by Storey *et al.*[9] using the quantized slab method, and compared to microwave absorption measurements. An improved method for determining the magnetostatic spectrum of rectangular ferromagnetic particles[10] has included the elliptical character of the mode precession and edge effects.

In the last few years extensive experimental work has been carried out to study the effects of lateral confinement on the dynamical properties of spin waves. In particular, the first Brillouin scattering observations of the discretization of the Damon-Eshbach (DE) mode[11] in magnetic micron-size Permalloy (PY) wires[12] and circular dots with a 2-micron diameter[13] have been reported. In the case of wires, the observed discrete spectrum was interpreted in terms of reso-

nanting standing waves within the wire. A quantitative interpretation of the circular dots spectrum, instead, was not possible because of the more complicated boundary conditions. However, it was noted that the measured frequencies were above that of the uniform precession mode (Kittel mode) of the corresponding ellipsoid, as expected for modes resulting from the discretization of the usual DE surface mode. Only one mode was found at a frequency below the Kittel mode, and it was supposed to be of backward magnetostatic nature. More recently, in a theoretical work by Guslienko and Slavin on the quantization of DE modes in tangentially magnetized circular dots[16] the measured frequencies of discretized DE modes were reproduced.

The aim of this paper is to investigate the dynamical properties of tangentially magnetized PY submicron-size cylindrical dots of different radii. The discretized spin-wave spectrum is investigated both theoretically and experimentally. For a deeper understanding of the character of the spin wave modes, measurements in two different scattering geometries, i.e., with the transferred wave vector parallel and perpendicular to the applied field **H**, respectively, have been performed.

The paper is organized as follows. In Sec. II the preparation of the sample and the experimental setup are described. Section III presents the experimental results, while the theoretical model used for the frequency calculation is presented in Sec. IV. Section V is devoted to a discussion of the results. Conclusions are drawn in Sec. VI.

II. SAMPLE PREPARATION AND EXPERIMENTAL SETUP

Squared arrays of cylindrical ferromagnetic PY ($Ni_{81}Fe_{19}$) dots were prepared using electron-beam lithography and electron-gun deposition in a vacuum of 1×10^{-8} Torr. Prior to deposition of the PY layer, the desired patterns were defined on thermally oxidized Si substrates capped by a layer of resist. The resist was removed by a lift-off process, and PY dots remained on the surface of the substrate. Several arrays of cylindrical dots were prepared with a fixed thickness $L=50$ nm and with radii of $R=100$, 200, 300, 400, and 500 nm. For all the samples the dot separation is equal to the diameter $2R$. Scanning electron microscopy and atomic force microscopy images confirmed that the morphology of the patterns was of good quality, concerning both dimensional control and uniformity.[17] Part of the magnetic film was left unpatterned to compare the consequences of patterning as measured by Brillouin light scattering (BLS). The BLS measurements were carried out at the GHOST laboratory, Perugia University,[18] using a Sandercock (3+3)-pass tandem Fabry-Perot interferometer[19] to analyze the frequency shift of light from a single-mode diode pumped solid state laser operating at $\lambda=532$ nm. The inelastically scattered light was sent through a crossed analyzer in order to suppress the background of elastically scattered light and surface phonons signal. As usual, a dc magnetic field, variable between 1 and 3 kOe, was applied in the sample plane and perpendicularly to the transferred wave vector scattering plane, i.e., in the DE geometry. These fields ensure the dots saturation for all the different radii investigated, as inferred by the shape of the Kerr effect loops.[20] The sample was mounted on a goniometer to allow rotation around the field direction, i.e. to vary the incidence angle of light, θ, between 8° and 70°. In addition, we took also measurements with the field parallel to the transferred spin-wave wave vector, in the so-called volume magnetostatic (BWVMS) spin-wave geometry, for a fixed angle of incidence $\theta=10°$. The amplitude of the spin-wave-transferred in-plane wave vector is related to the angle of incidence θ by the relation $q_{\parallel}=(4\pi/\lambda)\sin\theta$. Therefore, the wave vector interval investigated is in the range $(0.3–2.2)\times10^5$ cm^{-1}.

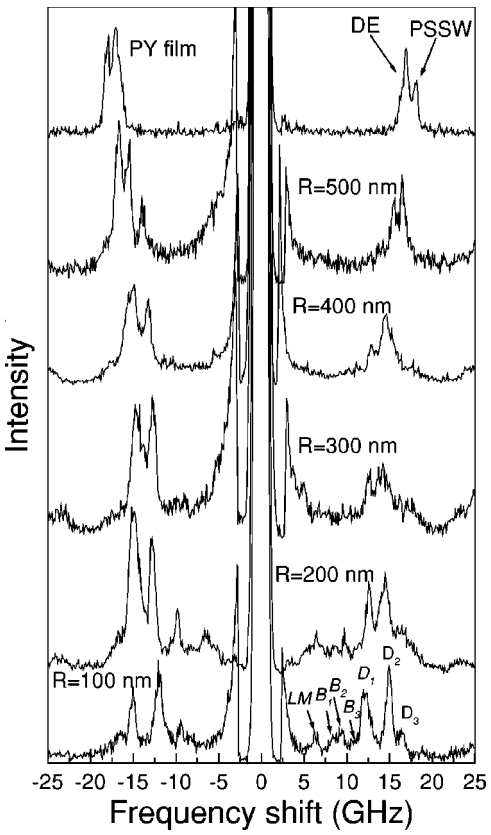

FIG. 1. Set of BLS spectra in the DE geometry of the PY cylindrical dots of different radius ($R=100–500$ nm) compared to the spectrum of the continuous film at $H=2$ kOe and $\theta=10°$. At $R=100$ nm *LM* labels the peak corresponding to the laterally localized mode; B_1, B_2, and B_3 indicate the peaks due to the backward modes corresponding to $n=1$, 2, and 3 nodes, respectively; D_1, D_2, and D_3 are the peaks which correspond to the three observed Damon-Eshbach like standing waves.

III. EXPERIMENTAL RESULTS

A complete set of experimental Brillouin spectra taken in the DE geometry, for a fixed value of the applied field $H=2$ kOe and of the incidence angle of light $\theta=10°$ ($q_{\parallel}=0.41\times10^5$ cm^{-1}), is shown in Fig. 1. In the spectrum of the continuous (unpatterned) PY film one can see peaks corresponding to the DE surface mode (16.7 GHz) and to the first perpendicular standing spin wave, at about 18 GHz. Instead, a number of discrete peaks corresponding to quantized

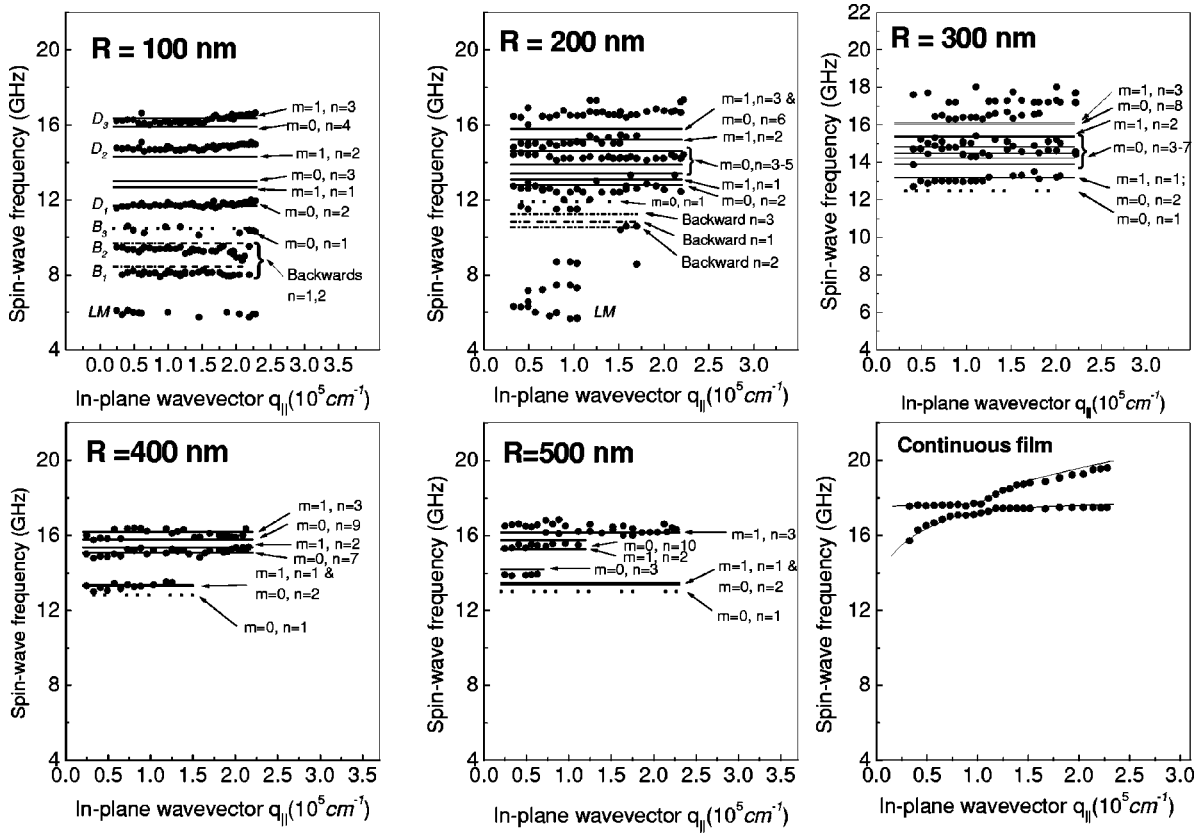

FIG. 2. Spin-wave frequencies vs transferred in-plane wave vector ($q_\parallel$) of the $R=100$–500 nm dot arrays for $H=2$ kOe together with the Damon-Eshbach and the first bulk perpendicular standing wave of the continuous film. Full circles: measured frequencies; continuous lines: calculated frequencies of the DE like waves; dash-dotted lines: calculated frequencies of the backward modes. The dotted line indicate the calculated frequency of the Kittel uniform mode ($m=0$, $n=1$).

modes is observable in BLS spectra taken from the patterned specimens. Interestingly, the number of resolved modes increases for dots with the smaller radius R. To identify the nature of the observed modes, their frequency dispersion with the angle of incidence θ, i.e., with the magnitude of the transferred wave vector $q_\parallel$, was investigated at a constant applied field. The results are displayed in Fig. 2 for the whole set of samples. It can be seen that all the modes are dispersionless, a typical behavior for confined modes. In more detail, one notes that the discretization is evident in the whole range of wave vector investigated only for specimens with smaller dots. In addition, in these specimens the number of detected modes is larger. As discussed in the next two paragraphs, the high-frequency modes [as a reference the frequency of the Kittel uniform precession mode $\nu_{\mathrm{Kittel}}=10.47$ GHz (Ref. 21) is represented by the dotted line in Fig. 2], can be classified as typical standing waves resulting from a discretization of the surface DE mode. With increasing radius, frequencies of these modes shift toward that of the DE one in the continuous film represented in Fig. 1 by the highest intensity peak at 16.7 GHz. Qualitatively, this frequency upshift can be attributed to a reduction of the in-plane static demagnetizing field with increasing dot radius. Concerning the low-frequency modes (indicated below by ν_{Kittel}), it is important to notice that they are only observed at low values of R (i.e., for $R=100$, and 200 nm). In addition, they are detectable in the whole $q_\parallel$ interval only for $R=100$ nm. This is an important characteristic which suggests that these modes can be interpreted as resulting from a discretization of backward modes. This kind of excitation in extended films has a wave vector parallel to the applied field, so it is not usually observed in BLS spectra taken in the DE geometry. However, in the case of very small magnetic dots, the lateral confinement breaks the translational symmetry and the wave vector conservation law, so that these modes can be detected. In particular, for each value of R, one can easily estimate which is the interval $\Delta q_\parallel$ where such modes are detected, according to the simple formula $\Delta q_\parallel \simeq 2\pi/2R$. Remarkably, one obtains that for $R=100$ nm, $\Delta q_\parallel = 3.2\times 10^5$ cm^{-1}, i.e., is larger than the experimentally accessible interval, while for $R=200$ nm $\Delta q_\parallel = 1.6\times 10^5$ cm^{-1}, in good agreement with the experiment (Fig. 2). For larger values of R the low-frequency modes are not experimentally detected due to the reduction of the $\Delta q_\parallel$ interval.

In order to achieve a direct proof of the above-mentioned character of the low-frequency modes, we measured Brillouin spectra in the BWVMS geometry, for both the continuous film and the patterned samples, as shown in Fig. 3. The spectra are recorded in the same experimental conditions ($H=2.0$ kOe and $\theta=10^{\circ}$) of those shown in Fig. 1. The band of the backward waves in the PY film presents its peak

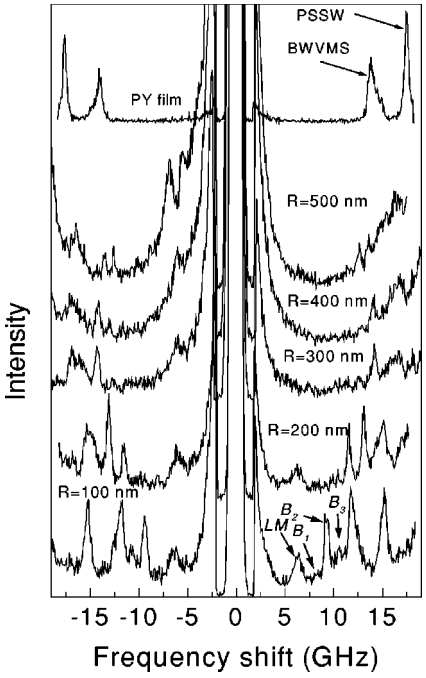

FIG. 3. Sequence of BLS spectra in the BWVMS geometry of the PY cylindrical dots of different radius ($R=100-500$ nm) compared to the spectrum of the continuous film at $H=2$ kOe and $\theta=10^{o}$. For the continuous film the backward peak is at 14.4 GHz. The meaning of the labels is the same as in Fig. 1.

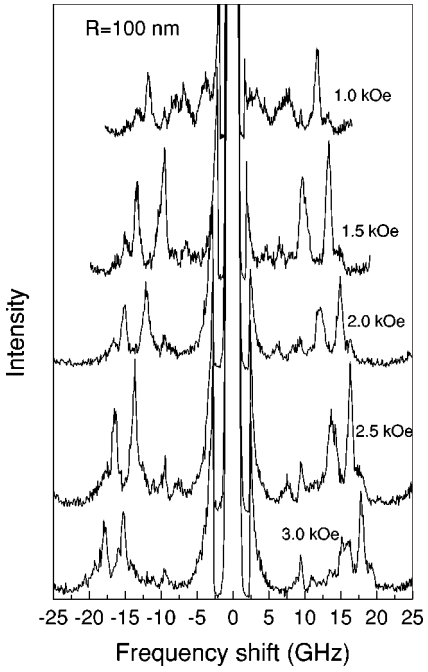

FIG. 4. Sequence of BLS spectra in the DE geometry for the saturated state for $R=100$ nm and at $\theta=10^{o}$ at different applied fields.

with a maximum at about 14.37 GHz. Different discrete peaks are present in the patterned samples and, in particular, the low frequency modes are also present in this experimental configuration at the same frequency values of those reported in Fig. 1. In order of increasing frequency, one finds the lowest laterally localized mode *LM*, which will be discussed in Sec. IV, and three backward volume modes (B_1, B_2, and B_3) observable on the anti-Stokes side of the spectra. In particular the mode *LM*, more visible by about 6 GHz on the Stokes side, is present in all these spectra. This confirms our hypothesis about the nature of these modes. One also notes that in the BWVMS geometry, in the case of the smaller dots, it is possible to observe three modes at larger frequency, coming from the splitting of the DE wave in the continuous film.

To complete the analysis of the spin-wave mode nature we have measured the dependence of the spin-wave frequency on the intensity of the external magnetic field for dots in the saturated state. A series of representative BLS spectra in the DE geometry for different applied fields at $R=100$ nm is shown in Fig. 4. The peaks corresponding to both DE and backward modes are clearly visible on both sides of the spectra, and are well resolved on the whole range of fields investigated. Figure 5 presents a summary of the measured frequencies as a function of the applied field for the different specimens.

IV. THEORETICAL MODEL

The treatment of spin waves in tangentially magnetized dots is a formidable problem which has not yet been solved completely. In general terms, the dynamical magnetization of a given mode should be a superposition of standing waves traveling at different angles with respect to a given in-plane direction, in particular that of the applied magnetic field. Second, the existence of laterally localized modes (i.e., edge modes) cannot be excluded, as in the case of rectangular dots or stripes.[14] However, a theory which encompasses all these features at the same time does not exist. Therefore, in order to provide at least a qualitative understanding of the BLS spectra, we restrict ourselves to particular models suitable for describing families of modes of an *a priori* defined character, in particular standing waves in the direction of the applied field (that we already called backward-like modes) and standing waves in the direction normal to it (Damon-Eshbach-like modes). Although this nomenclature is, strictly speaking, only valid for a system which is not laterally confined, we continue to adopt it in the present context in order to maintain a correspondence with the films. In the case of dots, modes which mix the above-mentioned characters are also certainly possible; however the BLS cross section for such standing waves, rapidly oscillating along several directions, should be smaller than that of the low-frequency lying backward and Damon-Eshbach modes, presenting only a few nodal surfaces. In fact, to a good approximation, the BLS scattering amplitude in small dots and in the long wavelength limit is simply proportional to the integral of combinations of the components of the dynamical magnetization.[15]

In order to quantitatively reproduce the experimental results relative to the surface dipole-exchange modes, their frequencies have been calculated in the framework of the Guslienko-Slavin model[16] applied to an isolated cylinder. As a matter of fact, the interdot magnetic coupling has been assumed negligible since the interdot distance $2R$ is larger

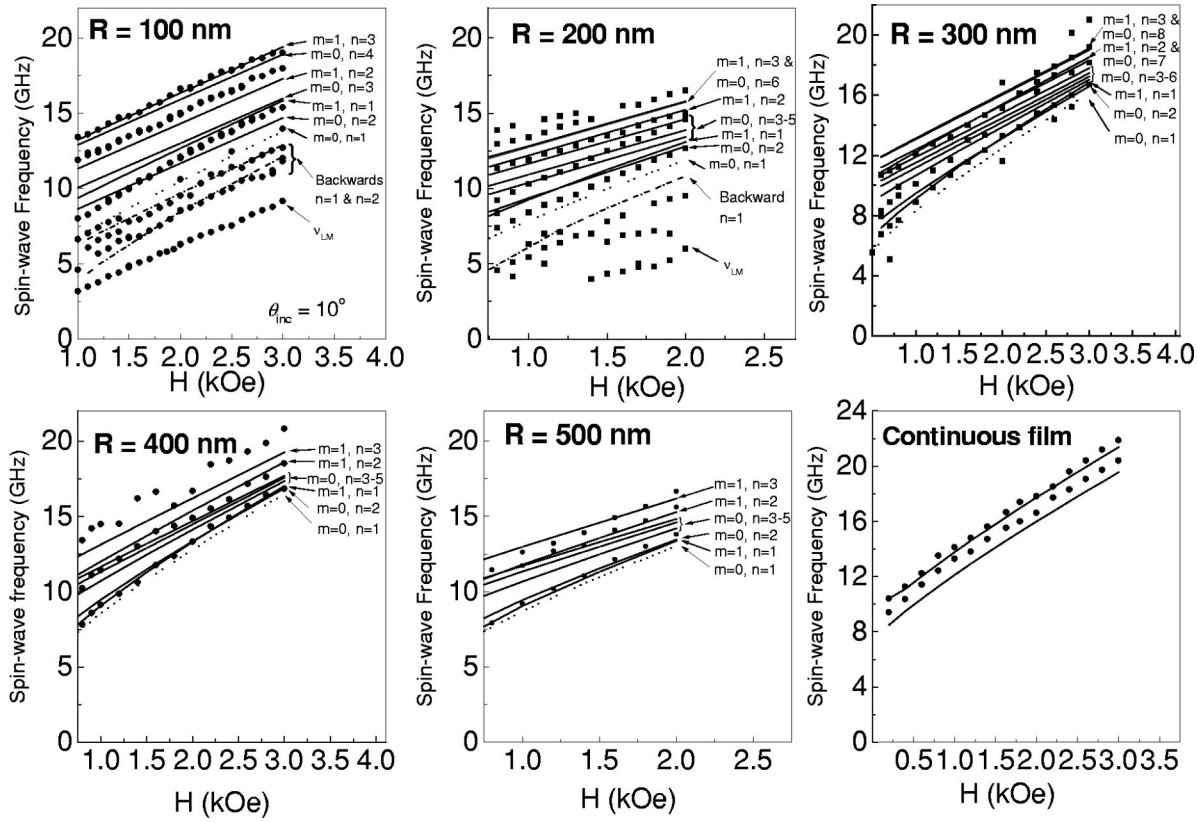

FIG. 5. As in Fig. 2, but as a function of the external field H. Dots are in the saturated state.

than the dot thickness L for the whole set of dots. In the calculations, the static magnetization **M** is assumed to be parallel to the in-plane y axis and uniform across the dot thickness (z direction). The eigenfunctions of the exchange operator, given by the in-plane and perpendicular components of the dynamic magnetization **m**, have the form of Bessel functions of the first kind J_m (the integer index $m=0,\pm1,\pm2,\ldots$ gives the order) times their corresponding angular functions of the kind $e^{im\phi}$ (ϕ is the in-plane angle). The radial boundary condition on **m** are imposed, supposing that no pinning is present on the lateral surface of the dots. The above-mentioned modes have frequencies larger than the resonant mode[21] which represents the lowest excitation and whose frequency in a particle of cylindrical shape and in-plane magnetization is given by: $\nu_{\mathrm{Kittel}}=\gamma/2\pi[H(H+4\pi M_s(1-3N_{\parallel})]^{1/2}$ where $N_{\parallel}$ is the effective in-plane demagnetizing factor.

Let us now come to a qualitative description of the low-frequency modes of the spectra, as the analogous of the backward magnetostatic waves of films[11,22,23] with an in-plane wave vector component along the direction of the external field **H** (y direction). Even if these modes have already been detected in dots of different shape,[13] up to now no quantitative comparison between experiments and calculations has been reported in the literature. As in the case of magnetic films we suppose that these modes are characterized by both perpendicular and parallel wave vector components, q_z and q_y, respectively. The introduction of the dependence of the dynamic magnetization on the q_z wave vector component is reasonable, especially for the low radii dots which may not be considered as thin dots. The in-plane wave vector q_y is quantized under the hypothesis of no pinning following the same approach already used in the case of DE modes. In this case we have used eigenfunctions in the form of stationary waves assuming a propagation along the y direction. For the whole set of backward volume modes the perpendicular wave vector q_z may be found from the transcendental equation[11]: $q_z\tan(q_zL/2)=q_y$.

The quantization of q_y leads to that of q_z, which is obtained numerically solving the above transcendental equation. We suppose that the whole set of backward modes belongs to the set of solutions related to the first branch of the function $q_z\tan(q_zL/2)$. An analytic formula which gives their frequencies is directly obtainable from the Landau-Lifshitz equation of motion:

$$-\frac{1}{\gamma}\frac{d\mathbf{M}}{dt}=\mathbf{M}\times\mathbf{H}^{\mathrm{eff}}, \tag{1}$$

where γ is the gyromagnetic ratio and $\mathbf{H}^{\mathrm{eff}}(\mathbf{r},t)$ is the effective field. To solve Eq. (1) we decompose the effective field into a static and a dynamic part, i.e., $\mathbf{H}^{\mathrm{eff}}(\mathbf{r},t)=\mathbf{H}+\mathbf{H}^{\mathrm{dem}}(\mathbf{r})+\mathbf{h}^{\mathrm{exch}}+\mathbf{h}(\mathbf{r},t)$, where **H**, $\mathbf{H}^{\mathrm{dem}}(\mathbf{r})$, $\mathbf{h}^{\mathrm{exch}}$, and $\mathbf{h}(\mathbf{r},t)$ are the applied, static demagnetizing, effective exchange, and dipolar dynamic fields, respectively. We also apply the linear approximation to the total magnetization in the form $\mathbf{M}(\mathbf{r},t)=\mathbf{M}_s+\mathbf{m}(\mathbf{r},t)$ with $\mathbf{M}_s$ the saturation magnetization and $\mathbf{m}(\mathbf{r},t)=\mathbf{m}_0e^{i\mathbf{q}\cdot\mathbf{r}}e^{i\omega t}$ the dynamic magnetization; $\mathbf{m}_0$, **q**, and **r** are the magnetization amplitude, the total wave vector, and the generic position vector, respectively.

We also assume that $\mathbf{H}^{\mathrm{dem}}$ depends only on the coordinate-dependent demagnetizing factor $N_y(\mathbf{r})$, y being the axis along which $\mathbf{H}$ is applied. Under this hypothesis the three Cartesian components of the internal field including the exchange term $\mathbf{H}^{\mathrm{i}}(\mathbf{r},t)=\mathbf{H}+\mathbf{H}^{\mathrm{dem}}(\mathbf{r})+\mathbf{h}^{\mathrm{exch}}(\mathbf{r},t)+\mathbf{h}(\mathbf{r},t)$ may be expressed, omitting the dependence on t, as

$$H_x^i(\mathbf{r})=h_x{}^{\mathrm{exch}}(\mathbf{r})+h_x(\mathbf{r}),$$

$$H_y^i(\mathbf{r})=H-4\pi N_y(\mathbf{r})M_s+h_y{}^{\mathrm{exch}}(\mathbf{r}), \tag{2}$$

$$H_z^i(\mathbf{r})=h_z{}^{\mathrm{exch}}(\mathbf{r})+h_z(\mathbf{r}),$$

where m_x and m_z are the components of the dynamic magnetization. In the magnetostatic approximation the amplitude $\mathbf{h}_0$ of the dynamic field may be expressed in terms of the dynamic magnetization amplitude $\mathbf{m}_0$ (Ref. 24) in the form $\mathbf{h}_0=-4\pi\mathbf{q}\cdot\mathbf{m}_0\mathbf{q}/\mathrm{q}^2$.

After averaging $N_y(\mathbf{r})$ along the x and z directions, we have solved Eq. (1) in terms of the dynamic magnetization amplitudes components, obtaining

$$i\frac{\omega}{\gamma}m_{x0}=(-4\pi M_s q_x q_z/q^2)m_{x0} -[H+\alpha M_s q^2-4\pi N_y(y)M_s+q_z^2/q^2]m_{z0},$$

$$i\frac{\omega}{\gamma}m_{z0}=[H+\alpha M_s q^2-4\pi N_y(y)M_s+q_x^2/q^2]m_{x0} +(4\pi M_s q_x q_z/q^2)m_{z0}, \tag{3}$$

where $q^2=q_x^2+q_y^2+q_z^2$ and α is the exchange stiffness constant. The vanishing of the coefficient determinant gives the frequency of the generic nth backward mode:

$$\nu_n=\frac{\gamma}{2\pi}\left[(H_i(y)+\alpha M_s q^2)\left(H_i(y)+\alpha M_s q^2 +4\pi M_s\frac{q_z^2+q_x^2}{q^2}\right)-(4\pi M_s)^2\frac{q_x^2 q_z^2}{q^4}\right]^{1/2}, \tag{4}$$

where $H_i(y)=H-4\pi N_y(y)M_s$ is the y-dependent internal field and q_x, q_y, and q_z are the quantized wave vector components defined above. In Eq. (4) the dependence on the in-plane q_x component is also included. However, due to their nature, the backward modes have a q_y wave vector component larger than the correspondent q_x; therefore, we have neglected the q_x dependence in the calculated frequencies. In the following $N_y(y)$ has been calculated generalizing the Joseph-Schlömann demagnetizing factor formalism valid for axially magnetized cylindrical dots[25] to cylindrical dots with in-plane magnetization.

At low wave vectors, due to the dipolar field, the frequency decreases with an increasing number n (in half dot) of nodes related to q_y. When the exchange field becomes important the behavior is inverted and the frequency increases with increasing the number of nodes.

The magnetic parameters used in the calculations have been extracted from a fit to the experimental frequencies of the DE, the first and second standing bulk modes of the continuous PY film. Therefore, we have used the following parameters: $4\pi M_s=9.5$ kOe, $\gamma/2\pi=2.996$ GHz/kOe, and $\alpha/4\pi=2.42\times10^{-13}$ cm^2. The continuous film fitting procedure has been carried out, taking into account the dispersion relation both as a function of the transferred wave vector $q_\parallel$ and the applied magnetic field.

V. DISCUSSION

Let us now discuss in some detail, in particular for the specimens with smaller dots size, how the spin-wave frequencies calculated using the models described above compare with those measured by BLS. A direct comparison for the whole set of samples as a function of $q_\parallel$ at $H=2$ kOe is shown in Fig. 2. For all the radii a calculation of the DE modes coming from the zeros of Bessel functions J_0 and J_1 has been carried out. The former type of solution (J_0) is axially symmetric, the latter (J_1) antisymmetric with respect to the plane normal to the dot surface and containing $\mathbf{H}$, as stated in Sec. IV. In the limit of small dots, we expect that only the symmetric modes give contribution to the scattering intensity, however in general also the J_1 modes may contribute.

In particular, in the dot with the smallest radius, $R=100$ nm, the three DE modes (D_1, D_2, and D_3) observed in Fig. 1 are in good agreement with some calculated from the zeros of the solutions related to the Bessel functions of the first kind, J_0 and J_1, as shown in Fig. 2. The experimentally observed backward modes at $H=2$ kOe present at 8.0 (B_1), 9.3 (B_2), and 10.5 (B_3) GHz are well fitted using Eq. (4). In the calculations we have supposed that these modes are affected by the internal field at the dot center, $H_i(y=0)$, which for $R=100$ nm turned out to be 872 Oe. The theoretical frequencies obtained taking into account the boundary condition on the q_y and q_z wave vector components are $\nu_1=8.46$ GHz for $n=1$ and $\nu_2=9.69$ GHz for $n=2$ for the two lowest modes. One notes for $R=100$ nm that the experimental B_3 mode is also well reproduced by the calculated uniform Kittel mode frequency in a circular cylinder ($\nu_{\mathrm{Kittel}}=10.47$ GHz). Nevertheless, since a well resolved peak is also present at the same frequency in the BWVMS geometry, as shown in Fig. 3, we believe that this mode presents a backward nature. Moreover, the ν_{Kittel} frequency is calculated in a first approximation neglecting the nonuniformity of the corresponding dynamic magnetization with a maximum in the center of the dot which would upshift the frequency to a value approaching that of the D_1 measured mode.

In order to assign the low-lying excitation measured at about 6 GHz we have applied the quantization condition for localized spin-wave states described in Ref. 14. Following this procedure we have obtained that this mode may exist in the spatial regions where the q_y component is real and has an exchange-dominated character corresponding to an internal field in the range $H_i=0-750$ Oe. The calculated region where it is strictly localized is $0.4<y/R<0.8$, but we have assumed that the localization of this mode also includes the region where the internal field is assumed to be equal to zero

near the dot boundary, i.e., for $0.8<y/R<1$. The resonance quantization condition gives a frequency of 7 GHz which overestimates the experimental frequency by about 1 GHz. The reason for this discrepancy may be due to the application of this condition on a submicrometric scale where this treatment is not completely valid. In fact, in any case the wavelength of the spin mode is of the same order of magnitude of the dimensions of the sample. Due to a low number of in-plane oscillations of the magnetization of this mode its contribution to the scattering cross section becomes relevant in both scattering geometries.

For $R=200$ nm the behavior of the DE modes is similar to that at $R=100$ nm. Instead, the more limited $q_{\parallel}$ range of existence of the backward modes is evident. In particular, the *LM* mode for $R=200$ nm is observable in a $q_{\parallel}$ range which is approximately half that for $R=100$ nm, because of the reduction of the $\Delta q_{\parallel}$ indeterminacy. One notes a remarkable difference when the dot radius increases above $R=200$ nm. No backward mode is observable in the $q_{\parallel}$ range investigated. Again, DE modes are well reproduced by the zeros of the Bessel functions J_0 and J_1.

Finally, concerning the frequency dependence on the intensity of the external field (Fig. 5), one can notice that the backward mode frequencies increase almost linearly with *H*, presenting a behavior which is very similar to that of the DE modes. The agreement between the calculated and experimental frequencies is fairly good, especially for the $R=100$ nm sample.

VI. CONCLUSIONS

The dynamical magnetic properties of cylindrical PY dots have been studied as a function of their diameter, in the submicron range. Both quantized dipole-exchange DE and backward modes have been observed in Brillouin spectra. The measured frequencies of the former modes have been theoretically reproduced by taking into account both zero and first order Bessel solutions.

The low-frequency modes are the analogous of the backward magnetostatic volume waves present in extended films. The dynamical properties of these modes are affected by a non uniform demagnetizing field and feel the boundary conditions on the wave vector components. These modes are well observable as resolved peaks in the spectra measured in the BWVMS geometry, but are also observable in the DE geometry for small dot radius. Using a resonance quantization condition we have found that the lowest mode of this family is a laterally localized excitation.

ACKNOWLEDGMENTS

The authors acknowledge Dr. S. Demokritov for helpful discussions. Support by the FIRB Project RBNE017XSW of Ministero Istruzione, Università e Ricerca is acknowledged.

[1] J.I. Martin, J. Nogues, Kai Liu, J.L. Vicent, and Ivan K. Schuller, J. Magn. Magn. Mater. **256**, 449 (2003).
[2] C.A. Ross, H.I. Smith, T. Savas, M. Schattenburg, M. Farhoud, M. Hwang, M. Walsh, M.C. Abraham, and R.J. Ram, J. Vac. Sci. Technol. B **17**, 3168 (1999).
[3] S. Demokritov and B. Hillebrands, in *Spin Dynamics in Confined Magnetic Structures I*, edited by B. Hillebrands and K. Ounadjela, Springer Series in Topics in Applied Physics (Springer-Verlag, Berlin, 2002), p. 65.
[4] L.R. Walker, Phys. Rev. **105**, 390 (1957).
[5] P.C. Fletcher and C. Kittel, Phys. Rev. **120**, 2004 (1960).
[6] R.I. Joseph and E. Schlömann, J. Appl. Phys. **32**, 1001 (1961).
[7] M. Sparks, Phys. Rev. B **1**, 3831 (1970).
[8] T. Yukawa and K. Abe, J. Appl. Phys. **45**, 3146 (1974).
[9] B.E. Storey, A.O. Tooke, A.P. Cracknell, and J.A. Przystawa, J. Phys. C **10**, 875 (1977).
[10] P.H. Bryant, J.F. Smith, S. Schultz, and D.R. Fredkin, Phys. Rev. B **47**, 11255 (1993).
[11] R.W. Damon and J.R. Eshbach, J. Phys. Chem. Solids **19**, 308 (1961).
[12] C. Mathieu, J. Jorzick, A. Frank, S.O. Demokritov, A.N. Slavin, B. Hillebrands, B. Bartenlian, C. Chappert, D. Decanini, F. Rousseaux, and E. Cambril, Phys. Rev. Lett. **81**, 3968 (1998); J. Jorzick, S.O. Demokritov, C. Mathieu, B. Hillebrands, B. Bartenlian, C. Chappert, F. Rousseaux, and A.N. Slavin, Phys. Rev. B **60**, 15194 (1999).
[13] J. Jorzick, S.O. Demokritov, B. Hillebrands, B. Bartenlian, C. Chappert, D. Decanini, F. Rousseaux, and E. Cambril, Appl. Phys. Lett. **75**, 3859 (1999); J. Appl. Phys. **87**, 5082 (2000).
[14] J. Jorzick, S.O. Demokritov, B. Hillebrands, M. Bailleul, C. Fermon, K.Y. Guslienko, A.N. Slavin, D.V. Berkov, and N.L. Gorn, Phys. Rev. Lett. **88**, 047204 (2002).
[15] J. Jorzick, S.O. Demokritov, C. Mathieu, B. Hillebrands, B. Bartenlian, C. Chappert, F. Rousseaux, and A.N. Slavin, Phys. Rev. B **60**, 15194 (1999).
[16] K.Yu. Guslienko and A.N. Slavin, J. Appl. Phys. **87**, 6337 (2000).
[17] T. Okuno, K. Shigeto, T. Ono, K. Mibu, and T. Shinjo, J. Magn. Magn. Mater. **240**, 1 (2002).
[18] http://ghost.fisica.unipg.it.
[19] J.R. Sandercock, in *Light Scattering in Solids III*, edited by M. Cardona and G. Güntherodt, Springer Series in Topics in Applied Physics, Vol. 51 (Springer-Verlag, Berlin, 1982), p. 173.
[20] G. Carlotti and G. Gubbiotti, J. Phys. C **14**, 8199 (2002).
[21] C. Kittel, Phys. Rev. **73**, 155 (1948).
[22] G. Gubbiotti, G. Carlotti, R. Zivieri, F. Nizzoli, T. Okuno, and T. Shinjo, J. Appl. Phys. **93**, 7607 (2003).
[23] M.G. Cottam and A.N. Slavin, in *Linear and Nonlinear Spin Waves in Magnetic Films and Superlattices*, edited by M. G. Cottam (World Scientific, Singapore, 1994), Chap. I, p. 29.
[24] C. Herring and C. Kittel, Phys. Rev. **81**, 869 (1951).
[25] R.I. Joseph and E. Schlömann, J. Appl. Phys. **36**, 1579 (1965).